FACULTY OF SCIENCE
PALACKÝ UNVERSITY OLOMOUC

Department of Optics

Tunable filters and variable interaction using polarization interferometers and liquid crystals

DIPLOMA THESIS

Vojtěch Krčmarský

2016

FACULTY OF SCIENCE
PALACKÝ UNVERSITY OLOMOUC

Department of Optics

Tunable filters and variable interaction using polarization interferometers and liquid crystals

DIPLOMA THESIS

Author:	Bc. Vojtěch Krčmarský
Study program:	N1701 Physics
Field of study:	Optics and Optoelectronics
Forma studia:	Full-time
Supervisor:	Mgr. Miroslav Ježek, Ph.D.

PŘÍRODOVĚDECKÁ FAKULTA
UNIVERZITY PALACKÉHO V OLOMOUCI

Katedra optiky

Laditelná filtrace a interakce v polarizačních interferometrech s tekutými krystaly

DIPLOMOVÁ PRÁCE

Vypracoval:	Bc. Vojtěch Krčmarský
Studijní program:	N1701 Fyzika
Studijní obor:	Optika a optoelektronika
Forma studia:	prezenční
Vedoucí diplomové práce:	Mgr. Miroslav Ježek, Ph.D.

Abstract

Polarization state control plays a crucial role in many quantum optics and quantum information experiments, where information is coded into polarization degree of freedom of light. The manipulation with polarization state and its measurement are inevitable parts of every such experiment. Standard methods for polarization state analysis require physical movement of quarter waveplates and half waveplates. This movement takes time proportional to an angle of rotation and brings some other issues.
In this Thesis, liquid crystal modules, based on simple liquid crystal displays are characterized and used to perform faster polarimetric measurements using minimal polarization tomography, phase modulation in the Mach-Zehnder interferometer, and polarization filtering. The absence of moving parts and fast voltage-dependent polarization transformation are biggest advantages of this approach.
Results, presented in this Thesis, show that liquid crystal modules, made of common liquid crystal displays, can work in quantum optics experiments as units for polarization state preparation and analysis. They can be used also in interferometers without destroying the interference.

Key words

Polarization, liquid crystals, liquid crystal module, polarization state analysis, polarimetry, minimal quantum state tomography, phase modulator, polarization filter

Poděkování

Poděkování. Poděkování. Poděkování. Poděkování. Poděkování. Děkuji mojí holce/klukovi že to se mnou vydržel(a). Poděkování. Poděkování. Poděkování. Poděkování. Poděkování. Poděkování. Poděkování. Poděkování. Poděkování. Poděkování. Poděkování. Poděkování. Poděkování. Poděkování. Poděkování.

Declaration

I declare that I have written Diploma Thesis "Tunable Filters and variable interaction using polarization interferometers and liquid crystals" on my own under the guidance of Mgr. Miroslav Ježek, Ph.D. by using theoretical resources, which are referred to in the list of literature. I agree with the further usage of this document according to the requirements of the Department of Optics.

In Olomouc on .....

.....

Vojtěch Krčmarský

Contents

Introduction

Quantum information processing became the merit of interest for its broad applications in secure communication, quantum metrology or quantum lithography [1]. Quantum information experiments could be performed on many platforms. Advanced experiments were performed with trapped ions [2], atoms, nuclear magnetic resonance, and photons [3]. New possibilities bring technologies, such as superconducting quantum circuits [4]. All these systems have their advantages and disadvantages[1, 3].

The quest of quantum information processing is to develop a quantum computer that provides us with ultrafast factoring and potential to perform simulations of quantum system dynamics [3]. The main requirements for the universal quantum computer were proposed by *DiVincenzo* in [5]. Quantum computing with photons satisfies most of these criteria.

Photons, as information carriers, interact with the surrounding environment weakly, but can be easily manipulated to create a quantum bit. In 2001 *E. Knill, R. Laflamme and G. J. Milburn* showed that linear optics is sufficient for quantum information processes with photons [6]. This discovery opened great interest in the quantum optics experiments.

Properties of photons enable performing experiments, such as long distance quantum teleportation, where current record distance is more than 100 km in optical fibre [7] and even in free space [8]. This was also used in the most recent test of Bell inequality [9].

Another large group of quantum information experiments deals with the construction of quantum logic gates. These gates use different degrees of freedom, such as its polarization, time-bin or path, to encode the information [10]. At the output of these experiments, the information has to be read out. For quantum bits encoded in polarization, it means to perform polarimetric measurements. The number of measurements increases exponentially with number of qubits processed in the experiment. This is a reason why developing faster polarization measurements is a of high importance.

A possible approach to speed up measurements is to use liquid crystals. The liquid crystal devices were used in quantum optics experiments, creating depolarization channels [11], quantum cryptography protocols [12], and others. This technology can find great application in quantum random walks on a photonic platform. A quantum random walk is an alternative approach for constructing quantum logic gates [13, 14] These experiments are

based on multiple path interferometers, where each path has to be addressed individually [15]. This is relatively difficult to perform with standard elements, such as quarter and half waveplates. On the other hand, custom design of liquid crystal module could make this task easy. Liquid crystals were also used in experiments as variable phase retarders, simulating rotational waveplate with voltage dependent retardation [16], polarization rotators [17], or polarization controllers [18, 19].

This technology finds application in many branches of optical experiments. Liquid crystals are, for example, broadly used in spatial light modulators. These devices are used for transformation of a wavefront of a light wave. Amazing application, such as vortex beams, can be created with these devices [20]. Another application can be found in digital holography [21]. The polarization properties of such device were analysed at our department by *J. Běhal* [22].

The aim of this Thesis is to show the possible application of the liquid crystal technology for quantum information processing and polarimetry. Three types of devices based on liquid crystal technology - units for polarization state preparation and analysis, polarization filter, and phase modulator - will be presented in this Thesis. The liquid crystal modules were made of liquid crystal displays available in almost any shop with electronic components. These devices can be directly used in quantum optics experiments.

1 Polarization of light

Let us consider a monochromatic plane wave with frequency ν and corresponding angular frequency $\omega = 2\pi\nu$ propagating in a direction of z axis with velocity c lies in the $x - y$ plane. The electric field is described by following equation:

$$\mathcal{E}(z,t) = \mathrm{Re}\left\{\mathbf{A}\exp\left[\mathrm{i}\omega\left(\mathrm{t} - \frac{\mathrm{z}}{\mathrm{c}}\right)\right]\right\}, \tag{1}$$

where $\mathbf{A} = A_x\hat{\mathbf{x}} + A_y\hat{\mathbf{y}}$ is a vector with complex components A_x and A_y[23]. To describe the polarization of this wave, we have to trace the endpoint of vector $\mathcal{E}(z,t)$ at point z as a function of time. Following formula describes the polarization ellipse [23–25].

$$\frac{\mathcal{E}_x^2}{a_x^2} + \frac{\mathcal{E}_y^2}{a_y^2} - 2\frac{\mathcal{E}_x}{a_x}\frac{\mathcal{E}_y}{a_y}\cos\varphi = \sin^2\varphi, \tag{2}$$

where $\varphi = \varphi_y - \varphi_x$ is a phase difference, $\mathcal{E}_x$ and $\mathcal{E}_y$ are x and y components of the electric field with amplitudes a_x and a_y respectively.

The orientation and shape of this ellipse, given by the phase difference φ and balance of amplitudes a_x and a_y, determines the polarization state of light. We talk about right elliptical polarization in case of rotation clockwise and in case of counter clockwise rotation, we talk about left elliptical polarization. In special cases, when $\varphi = 0$ or π, the polarization ellipse collapses into line and we talk about linear polarization. If phase difference $\varphi = \frac{\pi}{2}$ and $a_x = a_y$, the ellipse becomes a circle and we talk about right circular polarization. For $\varphi = -\frac{\pi}{2}$ and $a_x = a_y$, we talk about left circular polarisation.

1.1 Describing polarization

Jones vectors

Lets consider a plane monochromatic wave with frequency ν propagating along the z axis. This wave is fully characterized by the complex envelopes $A_x = a_x\exp(i\varphi_x)$ and $A_y = a_y\exp(i\varphi_y)$ of the x and y components of the vector of electric field. These complex amplitudes can be written as a column vector - Jones vector $\mathbf{J}$ [26],

$$\mathbf{J} = \frac{1}{\sqrt{A_x^2 + A_y^2}}\begin{pmatrix} A_x \\ A_y \end{pmatrix}. \tag{3}$$

Jones vectors are normalized such that $||\mathbf{J}|| = \mathbf{J}^\dagger\mathbf{J} = 1$, where $\dagger$ denotes Hermitian conjugation, and describe only pure polarization states [25].

For single photons, the Jones vectors can be interpreted in analogy with two level quantum system as a description of a pure quantum state $|\Psi\rangle$.

Stokes vectors

Every polarization state can be represented as a point in a space. Stokes vectors describe the polarization state with four numbers S_0, S_1, S_2, S_3. The parameter S_0 represents distance of a point from the origin of the coordinate system. The other three parameters are coordinates of a point in space, given by two angles χ and ψ:

$$S_1 = S_0 \cos 2\chi \sin 2\psi \tag{4a}$$

$$S_2 = S_0 \sin 2\chi \tag{4b}$$

$$S_3 = S_0 \cos 2\chi \cos 2\psi. \tag{4c}$$

From equations 4 it is obvious, that following is satisfied.

$$S_0^2 = S_1^2 + S_2^2 + S_3^2. \tag{5}$$

The parameter S_0 goes from 0 for completely unpolarized light to 1 for pure polarization states. Therefore, every polarization state can be geometrically represented on a sphere - Poincare sphere. Pure states lie on the surface of the sphere, while mixed states are inside the sphere. [23]. The Poincare sphere is depicted in Fig. 1.

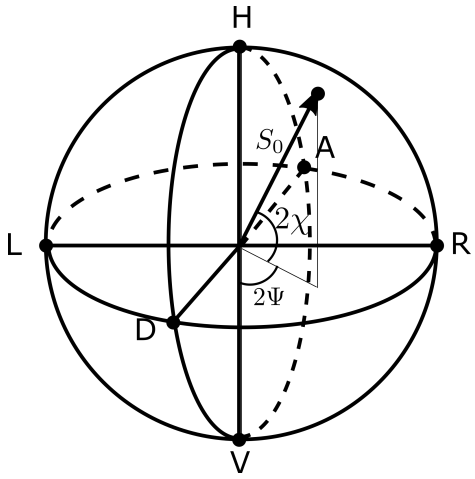

Figure 1: Poincare sphere.

Density matrix

This approach allows us to describe either pure states and mixed states equally. The density matrix is a 2×2 Hermitian matrix with $\mathrm{Tr}\left[\rho\right] = 1$. In analogy with the two level mixed quantum system, the polarization state can be represented as

$$\rho = \sum_k p_k \left|k\right\rangle \left\langle k\right|, \tag{6}$$

where p_k is the probability of finding the pure state $\left|k\right\rangle$ in the given mixture ρ. The density matrix can be also found using Jones vectors as

$$\rho = \left\langle JJ^{\dagger}\right\rangle = \begin{pmatrix} \left\langle U_x U_x^*\right\rangle & \left\langle U_x U_y^*\right\rangle \\ \left\langle U_y U_x^*\right\rangle & \left\langle U_y U_y^*\right\rangle \end{pmatrix}, \tag{7}$$

where $\dagger$ represents Hermitian conjugation and $*$ represents complex conjugation. U_x, U_y are elements of the Jones vector.

The density matrix is connected with Stokes parameters by following equation (8)

$$\rho = \frac{1}{2}\left(\sigma_0 + \sum_{i=1}^{3} S_i \sigma_i\right), \tag{8}$$

where S_i are Stokes parameters and σ_i are corresponding Pauli matrices:

$$\sigma_1 = \begin{pmatrix} 0 & 1 \\ 1 & 0 \end{pmatrix};\ \sigma_2 = \begin{pmatrix} 0 & -i \\ i & 0 \end{pmatrix};\ \sigma_3 = \begin{pmatrix} 1 & 0 \\ 0 & -1 \end{pmatrix};\ \sigma_0 = \begin{pmatrix} 1 & 0 \\ 0 & 1 \end{pmatrix}. \tag{9}$$

1.2 Describing transformation of polarization

Polarization of light wave could be transformed by many types of optical elements. The most common elements are based on birefringece or selective absorption. It is of high importance to describe the effect of such elements on the electric field of light, especially on its polarization.

Fully polarized light described by Jones vectors **J** is transformed by 2×2 matrices called Jones matrices. In analogy with a quantum information, the transformation of polarization could be treated as transformation of any other qubit [27]. The basic operations on quantum bits are based on Pauli matrices, presented in Eq. 9. A continuous family of single-qubit rotations could be achieved when Pauli matrices are exponentiated [27]. Any unitary transformation could be achieved by combining these matrices.

Following matrices define principal polarization transformations.

$$P = \begin{pmatrix} 1 & 0 \\ 0 & 0 \end{pmatrix}; R(\vartheta) = \begin{pmatrix} \cos\vartheta & \sin\vartheta \\ -\sin\vartheta & \cos\vartheta \end{pmatrix}; T(\Gamma) = \begin{pmatrix} 1 & 0 \\ 0 & \exp\{-i\Gamma\} \end{pmatrix}, \tag{10}$$

where P is a Jones matrix of linear polariser oriented along the x axis, $R(\vartheta)$ is matrix of rotation of angle ϑ and $T(\Gamma)$ is matrix of phase retarder with retardation Γ with optical axis parallel with the x axis.

The output polarization $\mathbf{J}_{\text{out}}$ after propagating through a system described by Jones matrix T is determined as follows.

$$\mathbf{J}_{\text{out}} = T \cdot \mathbf{J}_{\text{in}}, \tag{11}$$

where $\mathbf{J}_{\text{in}}$ is Jones vector of input polarization state. The matrix of a system T usually consists of multiple polarization elements. The matrix of the whole system is determined by matrix multiplying of elements in opposite order to their organisation in the experiment. For example, If light propagates first through element described by Jones matrix T_1 followed by element with Jones matrix T_2, then the matrix of the whole system will be $T = T_2 \cdot T_1$.

1.3 Polarization state tomography

The goal of the polarization state tomography is to determine polarization state of light, its density matrix. The unknown polarization state can not be determined with only one measurement, but a large ensamble of photons is required in the procedure. These photons are projected into multiple different polarization basis.
Four basis measurements are required for successful polarization state reconstruction. Three to find free parameters of the polarization state and the fourth to determine normalisation [28, 29].

The measured data have to be processed to receive the parameters of the unknown polarization state. We can use direct reconstruction procedure to estimate elements of the density matrix. This method uses measured data as mean values of density matrix in respect to given base Ψ_i. These represent probability of finding state in given projection

$$p_i = \langle \Psi_i | \, \rho \, | \Psi_i \rangle \, . \tag{12}$$

The elements of density matrix or Stokes parameters can be found by reverting the Eq. 12. This procedure is feasible and easy to implement. However, the disadvantage of this

procedure is that sometimes the reconstructed state is not physical [30].

Other method for finding parameters of the unknown state is using statistical treatment to solve the problem. The Maximum Likelihood (ML) method could be used for this purpose. The ML approach estimates the state as a whole and works with prior knowledge about relations between elements of the density matrix. Thanks to this, the positivity and trace normalization are guaranteed [30, 31]. The ML procedure reconstructs state that most likely give measured data. The core of the procedure is to maximize the likelihood functional

$$\mathcal{L}(\rho) = \prod_i p_i^{n_i} = \prod_i \mathrm{Tr}\left[\rho \Pi_i\right]^{n_i}, \tag{13}$$

where Π_i are positive-operator-valued measure (POVM) elements and ρ is desired density matrix of our unknown state. If we are measuring projections onto pure states Ψ_i, the POVM elements become equivalent to density matrices of those states, or projectors onto these states:

$$\Pi_i = |\Psi_i\rangle \langle \Psi_i| . \tag{14}$$

By taking into account Eq. 14, the maximum likelihood functional could be rewrote as

$$\mathcal{L}(\rho) = \prod_i \langle \Psi_i| \rho |\Psi_i\rangle^{n_i}, \tag{15}$$

where n_i is the the rate of detecting a particular outcome i [32]. Again, It represents probabilities of finding the state in given projection. Polarization state analysis using ML procedure is described in [32]. In this Thesis, the ML procedure is used to reconstruct polarization states.

1.4 Quantum process tomography

When studying quantum processes, or quantum channels, the information about arbitrary quantum state transformation in this channel is required. The quantum channels could be described by the completely positive maps. These maps take input state, described by the density matrix ρ_{in} ($\mathrm{Tr}[\rho_{\mathrm{in}}] = 1$), and transform it to the output state ρ_{out}. Since the map $\mathcal{E}$ operates from a space of states to another space of states, the trace preserving condition is required.

$$\mathrm{Tr}\left[\mathcal{E}(\mathrm{A})\right] = \mathrm{Tr}\left[\mathrm{A}\right]. \tag{16}$$

The map, usually called process matrix or Choi's matrix, has shape $2^{2N} \times 2^{2N}$, where N is number of qubits.

The aim of quantum process tomography is to characterize the quantum process by a sequence of measurements [33]. As a result, we get completely positive map of the quantum channel [33–35].

$$\rho_{\mathrm{IN}} \xrightarrow{\mathcal{E}} \rho_{\mathrm{OUT}} = \mathcal{E}\left[\rho_{\mathrm{IN}}\right]. \tag{17}$$

This operator $\mathcal{E}$ characterizes the effect on the system, coherent evolutions, decohering interactions, and losses [36]. For quantum filters and general quantum channels, the condition (16) is replaced with inequality

$$\mathrm{Tr}\left[\mathcal{E}(\mathrm{A})\right] \leq \mathrm{Tr}\left[\mathrm{A}\right]. \tag{18}$$

Process matrices presented in this Thesis were found using the ML procedure. This approach searches for a process that most likely gives measured data. The scheme of ML procedure for quantum processes is presented in [37] and it is based on maximizing the likelihood function

$$\mathcal{L}[\mathcal{G}] = \prod_{m=1}^{n} \left[\mathrm{Tr}\left(\Pi^{(\mathrm{m})}\rho_{\mathrm{out}}^{(\mathrm{m})}\right)\right]^{f_m}, \tag{19}$$

where n is number of different combinations of detected POVMs $\Pi^{(m)}$, $\rho_{\mathrm{out}}^{(m)}$ are output states and f_m is relative frequency of the combination $\left(\rho_{\mathrm{in}}^{(m)}, \Pi^{(m)}\right)$ in the dataset [37].

2 Nematic liquid crystal technology

In the field of common displays, present for example in digital watches, calculators, or, in a more complex way, in televisions or monitors, the most frequent technology is using properties of nematic liquid crystals.
Liquid crystal is a liquid phase of matter. Molecules of these substances have the orientation order similar to crystals, but their spatial order is similar to liquids [23, 38]. Molecules of the nematic liquid crystals form a "thread-like" structure [38] and maintain parallel orientation (see Fig. 2)[23, 38]. This molecular alignment causes that refractive index, electrical conductivity, etc. are different in direction of long axis and short axis of the "cigar-shaped" molecule [38].

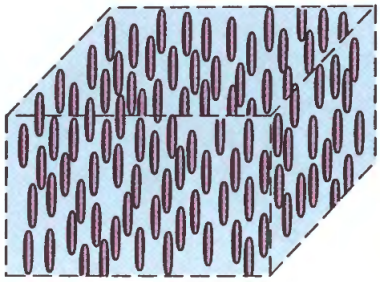

Figure 2: Parallel orientation of nematic liquid crystal (NLC) molecules [23].

The liquid crystal in typical LC displays is placed between two glass plates. These glass plates are on their inner sides covered by the electrodes made of a thin conducting layer of Indium Tin Oxide (ITO), and by an organic layer with linear micro-grooves. The second mentioned layer is called alignment layer and molecules of liquid crystals tend to place themselves into the grooves [38]. This sets the primary orientation of molecules along the thickness of the device. If the orientation of two alignment layers is parallel, we talk about nematic liquid crystal (NLC) device. The other option is that the alignment layers on the front and back glass plate are oriented perpendicularly. Since the molecules of nematic liquid crystal tend to orient themselves parallel to each other [38], the typical helical structure is created. In this case, we talk about a twisted nematic liquid crystal (TN LC) device.
The basic principle of a TNLC device operation is depicted in Fig. 3. In a state when a voltage is not applied on the device, the molecules of TN LC create helical structure. If linearly polarized light with plane of polarization parallel to orientation of the front

alignment layer enters this module, the polarization of the light wave follows the helical structure of TN LC molecules and the light on the output of the device is linearly polarized in direction of the alignment layer on the back side of the module (Fig. 3a). When one applies a voltage to the device, the molecules of the LC orient themselves along the electrical field. The light does not feel the birefringence property of the LC and thus, the polarization of the light is not changed (Fig. 3b).

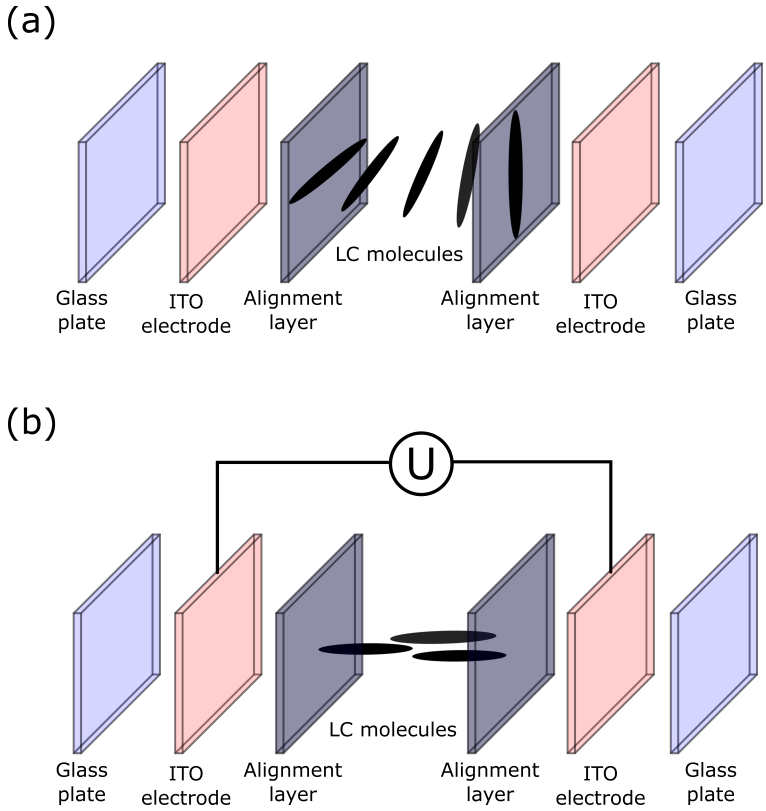

Figure 3: Basic structure and operational principle of a TN LC module. The module without applied voltage (a) nad with applied voltage (b).

Every LC module must be driven by a square wave signal with 0 V DC component. The DC component could damage the molecules causing malfunction of the device [39]. Any voltage connected with LC module referenced further in the text is mentioned as peak-to-peak value. Drawing of square wave signal is shown in Fig. 4

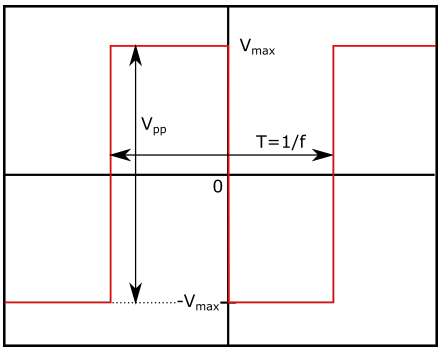

Figure 4: Driving voltage signal: V_{max} - amplitude; V_{pp} - peak-to peak voltage; T - period; f - frequency.

2.1 Used modules

For purposes of experiments presented in this Thesis, LC modules based on standard TN LC displays were used. The TN LC module is made from the single-character TN LC display type LUMEX LCD-S101D14TR. The schema and photo of this display is depicted in Fig. 5. The TN LC module is created from this display by removing all the polarization, reflective, and protective layers on the surface (Fig. 6a). The bare glass module is then properly cleaned so all the remains of adhesives are removed. Such element is then ready to use in experiment. For easy manipulation with these modules, I have affixed each LC element to the rotation stage. This allows to rotate the TN LC module in plane perpendicular to direction of propagating light. The TN LC module in rotation stage is shown in Fig. 6b.

This particular type of LC module has voltage range $(0 - 10)$ $\mathrm{V_{pp}}$. Measurements were performed with frequency of driving signal $f = 1$ kHz (T = 1 ms). The transmissivity of this module was determined as $T = 0.86$. The bare LC module is not covered with any anti-reflective layer. Schematic figure of TN LC module, further used in this Thesis, is depicted in Fig. 7. For driving LC modules, custom drivers constructed by Mgr. Michal Dudka, Ph.D. were used. Two generations of this driver were constructed.

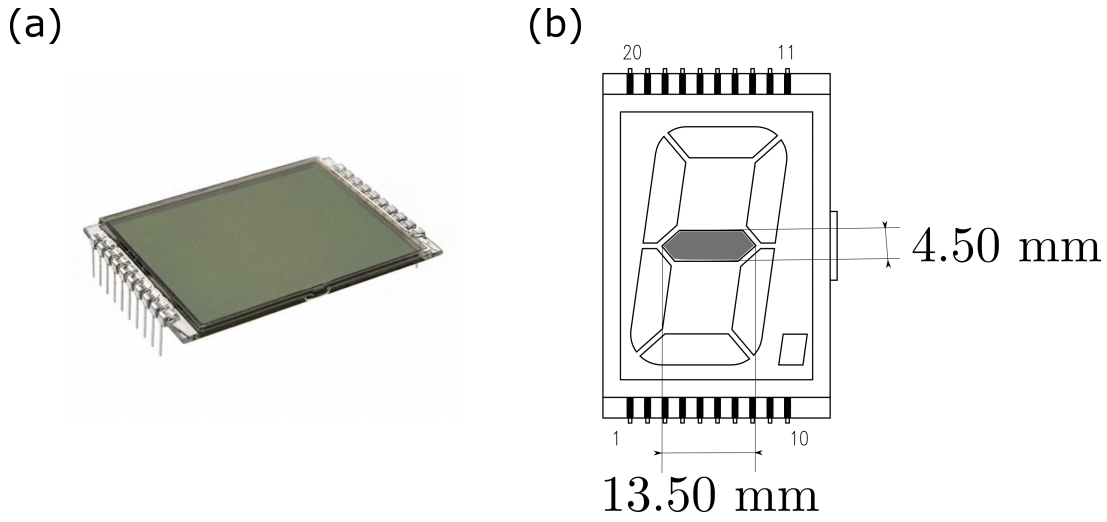

Figure 5: A photo of used TN LC display(a) and its scheme (b) with segment dimensions. Used segment is depicted as shaded region.

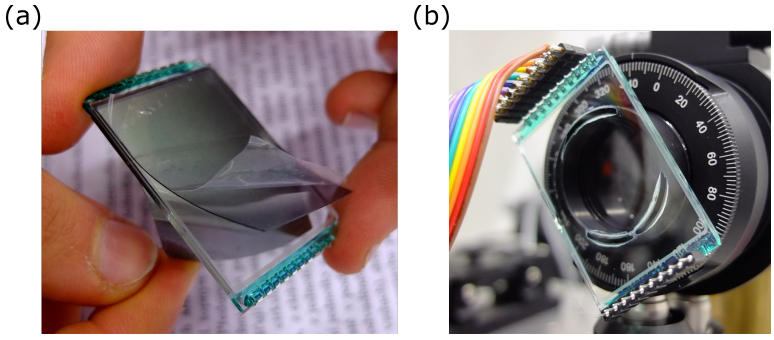

Figure 6: a) Photo of used TN LC display with partially removed polarization, reflection and protective layers. b) Photo of TN LC module in rotation stage placed in experimental setup.

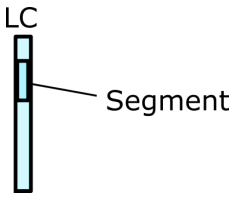

Figure 7: Schematic figure of TNLC module used in this Thesis. Segment means voltage-dependent area of the module.

3 Theoretical model

The impact of a TN LC device on polarization state of light can be described using the Jones formalism. The matrix of TN LC device could be derived using a sequence of infinitesimal polarization rotators and retarders[40–43] as:

$$J_{\mathrm{TNLC}} = \begin{pmatrix} \cos\varphi & -\sin\varphi \\ \sin\varphi & \cos\varphi \end{pmatrix} \begin{pmatrix} \cos\chi - i\frac{\delta}{2\chi}\sin\chi & \frac{\varphi}{\chi}\sin\chi \\ -\frac{\varphi}{\chi}\sin\chi & \cos\chi + i\frac{\delta}{2\chi}\sin\chi. \end{pmatrix} \tag{20}$$

In this matrix, φ is a total twist angle and δ stands for difference of ordinary and extraordinary refractive index of the LC (retardance). Parameter χ relates retardation δ and twist angle φ by formula $\chi^2 = \varphi^2 + \left(\frac{\delta}{2}\right)^2$.
The retardance δ is parameter dependent on voltage applied to the LC module.

Fig. 8 shows typical dependence of retardance on applied voltage. This data were provided by ThorLabs company for their LC modules. As it is obvious from the graph, the dependence is strongly nonlinear. The image shows, that until certain voltage ("threshold" voltage), the retardance is constant. After passing the threshold voltage, the retardation rapidly decreases and for higher voltages, the decrease slows. Some authors describe this function with the arctan [44]. However, the arctan function has symmetric shape. Thus, it can not describe the asymmetry of curve presented in Fig. 8. In this Thesis, the logistic function is used to model the dependence of retardance on applied voltage given by following formula:

$$\delta\left(V\right) = a + \frac{1}{b + \exp\left(d - cV^e\right)}, \tag{21}$$

where V is voltage applied on the module and a, b, c, d and e are parameters.

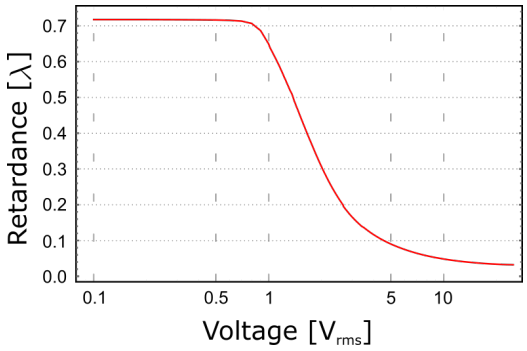

Figure 8: Dependence of retardance on applied voltage of LC device for laboratory use [45].

4 Single module characterization

If we want to work with TN LC modules, make combinations of them in more complex setups, and stack them into units, It is important to predict the polarization transformation of one module. For this purpose, the transformation of one TN LC module was measured. The experimental setup for this experiment is depicted in Fig. 9. The horizontally polarized light propagated through one segment of the LC module and output polarization was measured. This measurement was performed for various voltages applied to the module. This experiment is described in depth in [46]. The whole procedure was repeated for a rotated LC module. During the experiment, the transformation was measured for 3 angles of rotation ($\alpha_1 = 0°, \alpha_2 = 15°, \alpha_3 = 30°$). For each angle 200 voltages from interval $\langle 0, 10 \rangle$ V_{pp} were applied to the module. Results were fitted with the theoretical model consisting of matrix of the LC module (20) surrounded from both sides by a rotation matrix as

$$J_{\mathrm{TOT}} = R\left(-\vartheta - \alpha_i\right) \cdot J_{\mathrm{TNLC}} \cdot R\left(\vartheta + \alpha_i\right). \tag{22}$$

The additional rotation by angle ϑ was added to the model to determine the initial rotation angle and sign convention of rotation. Angles $\alpha_i; i = \{1, 2, 3\}$ in (22) are known rotation angles. As theoretical model of dependence of retardation $\delta(V)$ on applied voltage, the Eq. (21) was used.

Results of this experiment are depicted in Fig. 10 as colour dots. Experimental data were

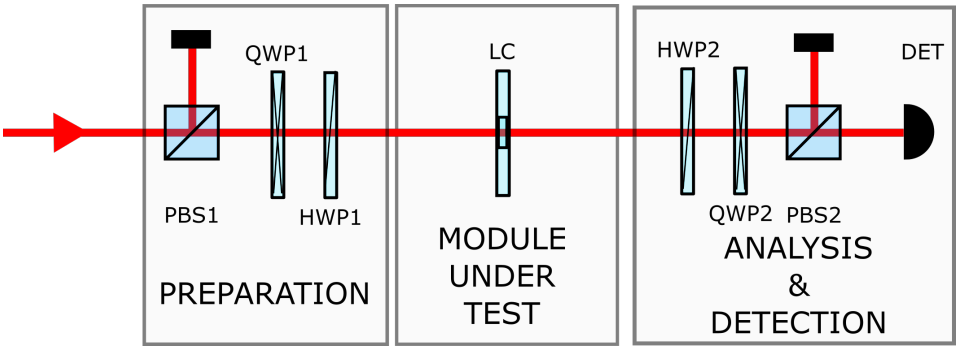

Figure 9: Scheme of exerimental setup for characterization of one LC module: polarization beamsplitter (PBS), quarter waveplate (QWP), half waveplate (HWP); LC module (LC), detection (DET). Detection part in this case consists of coupling into single mode optical fibre and decoupling in front of the PIN diode, where the signal is detected.

fitted using the least squares procedure by searching for values of parameters minimizing

the following formula:

$$\sum_{l=\alpha_1,\alpha_2,\alpha_3} \sum_{m=1}^{3} \sum_{n=1}^{N} \left(S_{m,n,l} - T_{m,n,l}\right)^2 , \tag{23}$$

here $S_{m,n,l}$ is m^{th} Stokes parameter of measured output state when n^{th} voltage was applied to the module rotated by angle l. $T_{m,n,l}$ is theoretical model for each $S_{m,n,l}$. Data for all three rotation angles were fitted at once.

Fitted parameters are $\varphi = 65.8°$, $\vartheta = 57.6°$. Fitted dependence of retardance on applied voltage is depicted in Fig. 11.

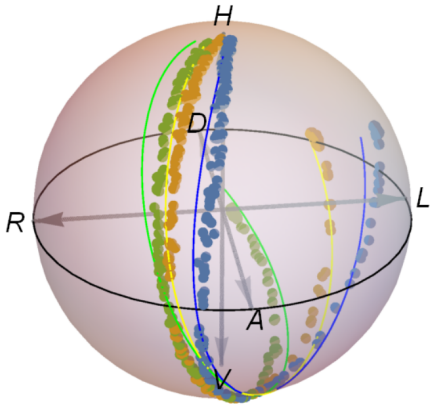

Figure 10: Transformation of a horizontally polarized light by a single TN LC module: blue dots - rotation angle $\alpha_1 = 0°$, yellow dots - rotation angle $\alpha_2 = 15°$, green dots - rotation angle $\alpha_3 = 30°$. Solid lines represent theoretical fit.

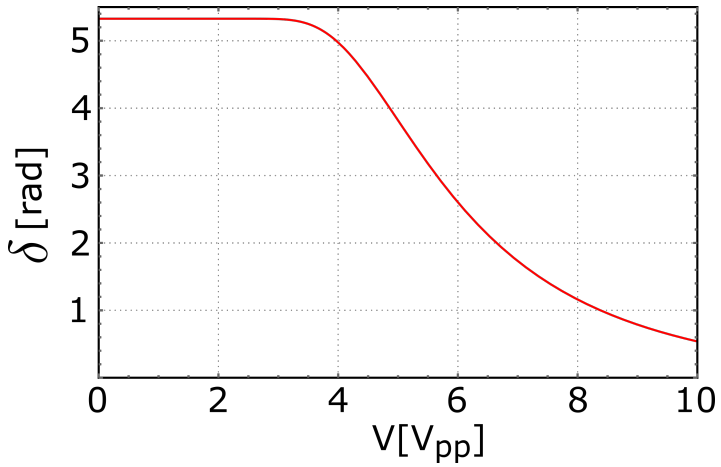

Figure 11: Fitted dependence of retardation δ on voltage.

5 Polarization state preparation and analysis using LC modules

5.1 Minimal quantum state tomography

Many quantum information experiments based on photonic platform use polarization degree of freedom to encode the information. To gain the information, the polarization state has to be analysed. This could be performed in many ways. In our laboratory, the polarization state analysis is usually done by projecting the state onto six basis polarization states (H, V, D, A, R and L). Projections are set using rotating quarter- and half-waveplates and a fixed polariser or PBS. The intensity or photon count rate is measured. This measurement represents probability of finding the photon in projected state. These probabilities are used to estimate the polarization state. The estimation is done using the maximum-likelihood procedure described in Sec. 1.3.

To determine the polarization state of light, at least four projections need to be done (see Sec. 1.3). The main idea of minimal quantum state tomography is to find four linearly independent states that decompose unit. Geometrically speaking, these four states create corners of an regular tetrahedron inside the Poincare sphere with its corners on the surface of the sphere. The four states define POVM elements for the minimal four-state tomography. These POVM elements creates symmetric informationally complete POVM [47]. Thus, following equation is satisfied.

$$\sum_{j=1}^{4} \Pi_j = 1, \tag{24}$$

where Π_j are POVM elements.
To reconstruct the polarization state, the maximum-likelihood method can be used. In the procedure, the reconstructed density matrices of the four (pure) states creating the optimal tetrahedron are used as projectors.

The optimal regular tetrahedron, created by the four ideal states, takes maximal volume of the Poincare sphere, that is $V_{\text{opt}} = \frac{1}{6\sqrt{2}} \left(\sqrt{\frac{8}{3}}\right)^3$. This volume can be used as a measure of a quality of found tetrahedron.
We can prepare states creating optimal tetrahedron using TNLC modules. The experiments with one such element were performed by *A. Peinado et al.* in [48]. They used the LC modules in various combinations with QWPs, linear polarisers, and mirrors to perform polarimetric measurements. There were also other experiments dealing with minimal state

tomography. For example *A. Ling et. al.* in their experiments presented in [49] introduced the tetrahedron quantum state tomography without moving parts. The principle of their experiment was to prepare projections into four states using series of polarization beamsplitters and fixed waveplates. On four photodetectors, they measured required projections simultaneously. The advantage of this method is that required projections are measured instantaneously. On the other hand, this approach is applicable only for polarization state analysis and not for polarization state preparation.

5.2 Experiments

First, the experimental setup was built with polarization state preparation and analysis using half- and quarter- waveplates. The scheme of experimental setup is depicted in Fig. 12. The main purpose to perform this experiment was to obtain data for later comparison of the traditional waveplate method and the LC method.

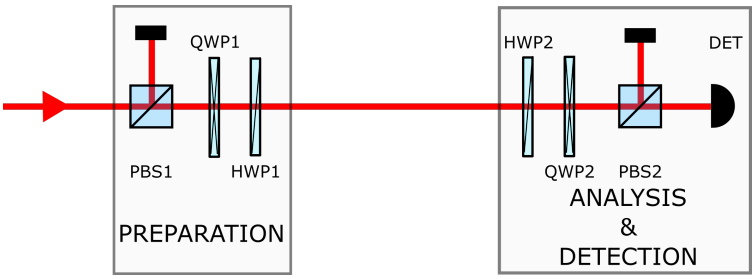

Figure 12: Scheme of experimental setup for polarization state preparation and analysis - waveplate preparation and analysis: polarization beamsplitter (PBS), half waveplate (HWP), quarter waveplate (QWP), detection (DET).

The beam was guided to the experiment from laser diode by the optical fibre. The part of this fibre was mounted in polarization controller used for total intensity adjustment. The light was then decoupled by collimator. The light propagated through the polarizing beam splitter PBS1 and the transmitted horizontal polarization was transformed by a series of quarter-waveplate QWP1 and half-waveplate HWP1. These prepare arbitrary polarization state. Afterwards, the polarization state was analysed with the half-waveplate HWP2, quarter-waveplate QWP2, and polarization beamsplitter PBS2. Finally, the light was coupled into a single-mode optical fibre and decoupled in front of the PIN diode detector. The experimental setup was built symmetrically, so the light could propagate in either directions and waveplates QWP2 and HWP2 can work as polarization state preparation.

The 6 basis states H, V, D, A, R, and L were prepared and reconstructed in this experimental setup and the process matrix of a free space was reconstructed using the maximum likelihood procedure. The reconstructed polarization states are shown in Tab. 1 and the reconstructed process matrix is depicted in Fig. 13. The reconstructed process has purity $P_{\mathrm{WP}} = 1.000$ and fidelity with theoretical matrix $F_{\mathrm{WP}} = 0.9986$. The fidelity was calculated using formula:

$$F = \mathrm{Tr}\left[\mathrm{M_{id}M_{ex}}\right], \tag{25}$$

where M_{id} is idal matrix and M_{ex} is experimental matrix.

	H	V	D	A	R	L
S_1	-0.038	0.036	0.999	-0.997	-0.043	0.075
S_2	-0.031	0.033	0.041	-0.069	0.998	-0.997
S_3	0.999	-0.999	0.022	-0.034	0.056	0.027
DOP	1	1	1	1	1	1

Table 1: Reconstructed states - wave-plate preparation and analysis

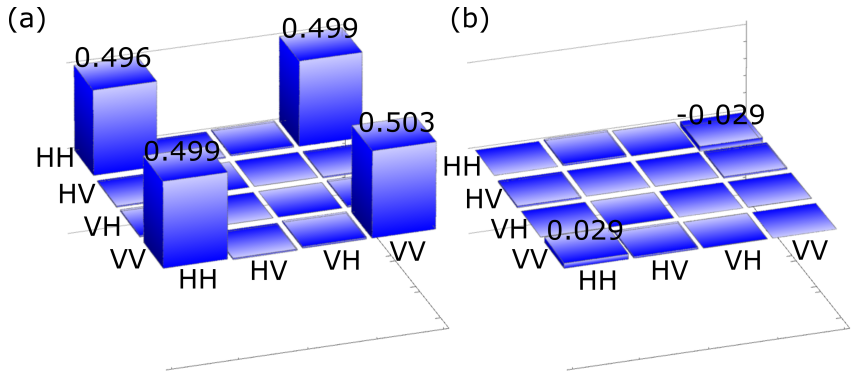

Figure 13: Reconstructed process matrix of free space: real (a) and imaginary (b) parts of the Choi matrix. States prepared and analysed with PBSs, HWPs and QWPs. Purity and fidelity of this process are $P_{\mathrm{WP}} = 1.000$ and $F_{\mathrm{WP}} = 0.9986$, respectively.

After this measurement, the waveplates on polarization state preparation were replaced by the sequence of two LC modules assembled into LC unit (LC PA unit 1). A photo and scheme of this unit is shown in Fig. 15. Scheme of the experimental setup is illustrated in Fig. 14 The optimal angles and voltages to set the optimal tetrahedron for analysis were found. These values are summarized in the Tab. 2.

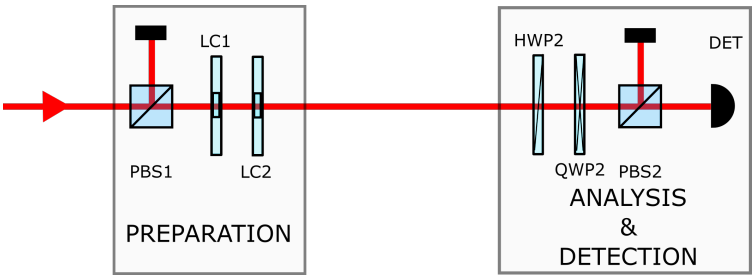

Figure 14: Scheme of experimental setup for finding the optimal tetrahedron for LC PA unit 1. LC PA unit 1 prepared polarization states analysed with waveplate analysis: polarization beamsplitter (PBS), half waveplate (HWP), quarter waveplate (QWP), detection (DET), LC modue (LC).

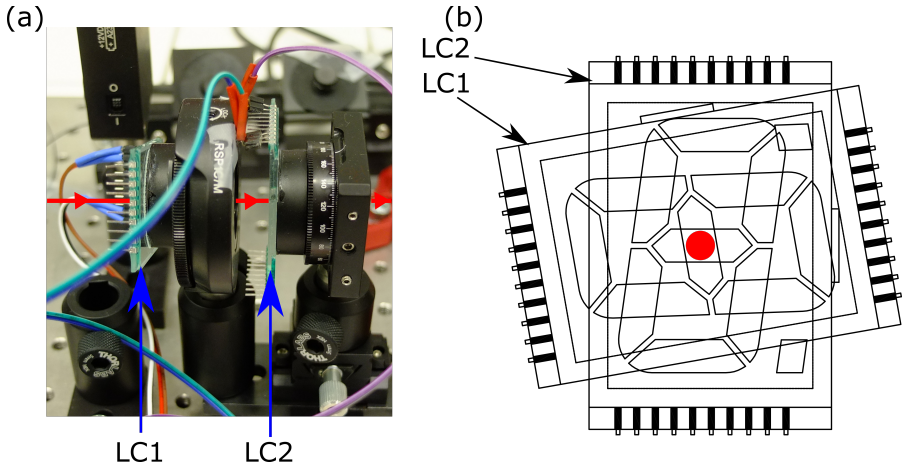

Figure 15: A photo of LC PA unit 1 (a). Red line represents propagating beam. Schema of LC PA unit 1 - front view (b). Red dot represents laser beam. It goes through an intersection of active segments of both LC modules.

Reconstructed polarization states creating corners of the tetrahedron are in Tab. 3. The tetrahedron is shown on Poincare sphere depicted in Fig. 16. Volume of the tetrahedron is $V_{\text{tet1}} = 0.998\ V_{\text{opt}}$.

Reconstructed density matrices of states $\Psi_1 - \Psi_4$ were used as projectors in the maximum likelihood procedure and the experiment was reconfigured.

Next, the direction of light propagation was reversed. HWP2 and QWP2 now prepared the polarization state and LC PA unit 1 reconstructed the polarization state (scheme in Fig. 17). Results of 6 basis states (H, V, D, A, R and L) reconstruction are in Tab. 4.

As we can see, the polarization state analysis using the LC PA unit 1 works sufficiently

	ϑ [°]	$V_{\Psi 1}$ [V_{pp}]	$V_{\Psi 2}$ [V_{pp}]	$V_{\Psi 3}$ [V_{pp}]	$V_{\Psi 4}$ [V_{pp}]
LC 1	85.5	8.18	8.54	5.42	3.75
LC 2	-33.0	6.85	4.75	4.54	9.91

Table 2: Orientation and voltages for reaching the optimal tetrahedron - LC PA unit 1

	Ψ_1	Ψ_2	Ψ_3	Ψ_4
S_1	0.763	0.275	-0.827	-0.224
S_2	-0.223	-0.117	-0.530	0.965
S_3	0.606	-0.954	0.185	0.138
DOP	1	1	1	1

Table 3: Polarization states creating optimal tetrahedron prepared by LC PA unit 1 and reconstructed with waveplates.

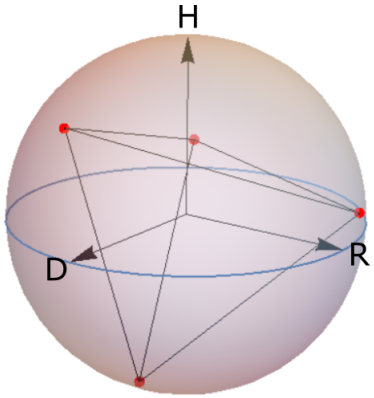

Figure 16: Polarization states (red dots) on Poincare sphere creating optimal tetrahedron generated by LC PA unit 1.

well. If we compare the output states with ones achieved by conventional method of polarization analysis, we can see, that "LC-based' analysis gives even better results than the conventional method.

After the first LC unit was calibrated and tested in the experiment, the second one was constructed. For further applications, it was important to have a possibility to propagate two beams through one segment. Therefore, the second LC PA unit (LC PA unit 2) was built using two parallel-oriented LC modules with horizontally aligned segments. The

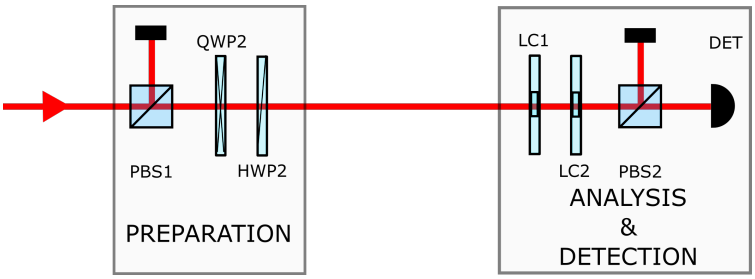

Figure 17: Scheme of experimental setup for polarization state preparation and analysis - waveplate preparation and analysis with LC PA unit 1: polarization beamsplitter (PBS), half waveplat (HWP), quarter waveplate (QWP), detection (DET), LC moule (LC).

	H	V	D	A	L	R
S_1	0.000	-0.011	1.000	-0.998	-0.048	-0.042
S_2	-0.042	-0.023	0.000	-0.065	-0.996	0.998
S_3	0.999	-1.000	0.023	-0.009	-0.068	-0.043
DOP	1	1	1	1	1	1

Table 4: Reconstructed basis states: wave-plate preparation and analysis using LC PA unit 1.

additional QWP was placed between them. Photo and schema of this unit is depicted in Fig. 18 The unit was characterized and optimal tetrahedron, with volume $V_{\mathrm{tet2}} = 0.993\, V_{\mathrm{opt}}$ was found. Tab. 5 shows Stokes parameters of states creating the optimal tetrahedron. This tetrahedron is also depicted on Poincare sphere in Fig. 19.

	Ψ_1	Ψ_2	Ψ_3	Ψ_4
S_1	0.321	0.591	-0.953	0.072
S_2	-0.898	-0.323	0.031	0.654
S_3	-0.301	0.739	0.301	-0.753
DOP	1	1	1	1

Table 5: States creating optimal tetrahedron prepared by LC PA unit 2 and reconstructed by LC PA unit 1.

The combination of the two LC units was then used to perform reconstruction of process matrix of a free space. Scheme of this experimental setup is shown in Fig. 20. The reconstructed matrix of process is depicted in Fig. 21

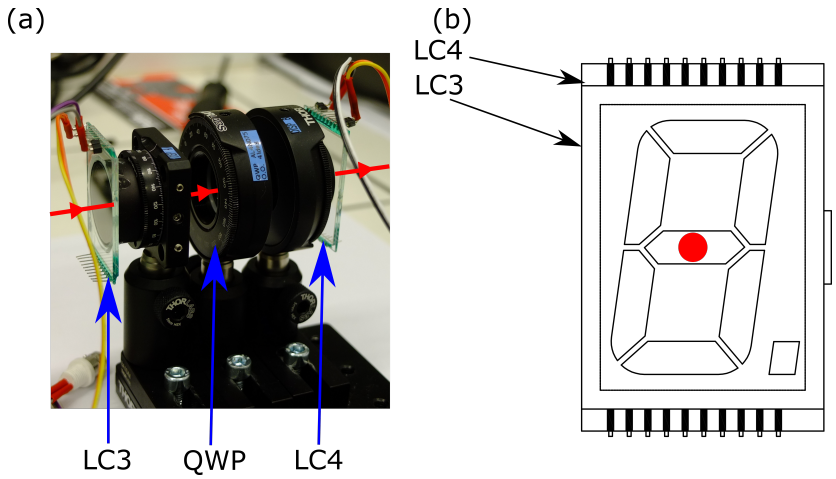

Figure 18: A photo of LC PA unit 2 (a). Red line represents propagating beam. Scheme of LC PA unit 2 - front view (b). Red dot represents propagating beam. It goes through an intersection of active segments of both LC modules. LC modules are aligned so in front view it looks like one module.

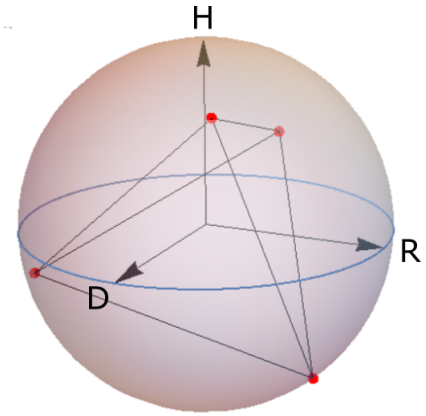

Figure 19: Polarization states (red dots) on Poincare sphere creating optimal tetrahedron generated by LC PA unit 2.

As we can see, the reconstructed process matrix is in agreement with expected matrix. The "corner" elements of a real part of the matrix are well balanced and they differ from ideal value by 0.004 in the worst case. The imaginary part is non-zero, but absolute values of all elements are below 0.02. The purity of the reconstructed process is $P_{\mathrm{LC}} = 1.000$ and fidelity is $F_{\mathrm{LC}} = 0.9993$.

We can compare results achieved by the conventional method, that is depicted in Fig. 13 and the result achieved with the polarization prepared and reconstructed using LC units

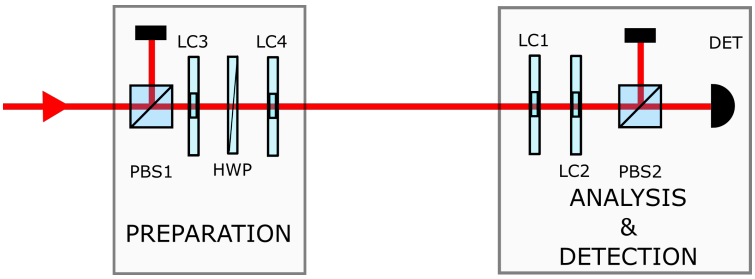

Figure 20: Scheme of experimental setup for polarization state preparation and analysis - LC preparation and analysis: polarization beamsplitter (PBS), quarter waveplate (QWP), detection (DET), LC moule (LC).

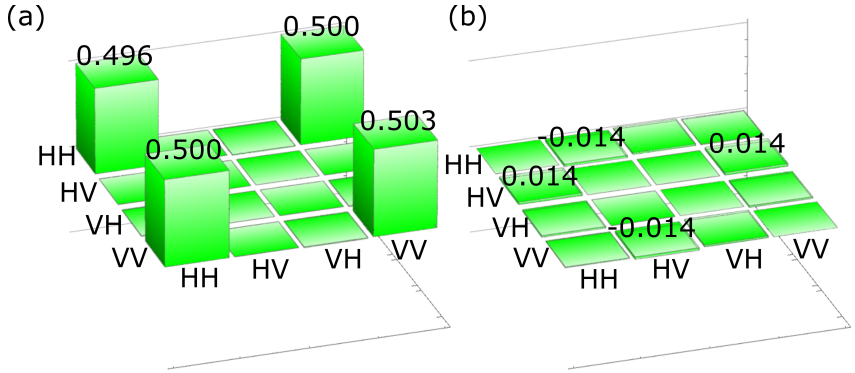

Figure 21: Reconstructed process matrix of free space: real (a) and imaginary (b) parts of the Choi matrix. The measurement was performed with LC unt 2 on state preparation and LC unit 1 on analysis. Purity and fidelity of this process are $P_{\mathrm{LC}} = 1.000.$ and $F_{\mathrm{LC}} = 0.9993$, respectively

depicted in Fig. 21. While purities of both matrices are the same, fidelities show that matrix achieved using the LC modules is slightly better ($F_{\mathrm{WP}} = 0.9986; F_{\mathrm{LC}} = 0.9993$).

The process matrix of a quarter waveplate oriented to its optical axis was also reconstructed using the two LC units as polarisation state preparation and analysis. The tested quarter waveplate was placed between the polarisation state preparation and analysis, as shown in Fig. 22.

The outcome process matrix of this measurement is depicted in Fig. 23. Purity of the process is $P_{\mathrm{QWP}} = 1.000$ and process fidelity is $F =_{\mathrm{QWP}}= 0.995$. These values show that either polarization state preparation and analysis work well. The imbalance of the process matrix could be caused by imperfections of tested QWP.

One of the reasons to use LC modules for polarization state preparation and analysis is

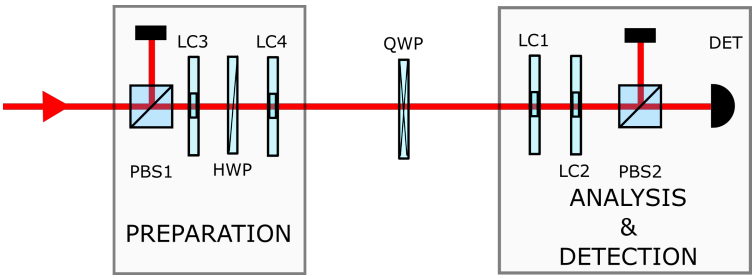

Figure 22: Scheme of experimental setup for measurement of process matrix of QWP using LC preparation and analysis: polarization beamsplitter (PBS), quarter waveplate (QWP), detection (DET), LC moule (LC).

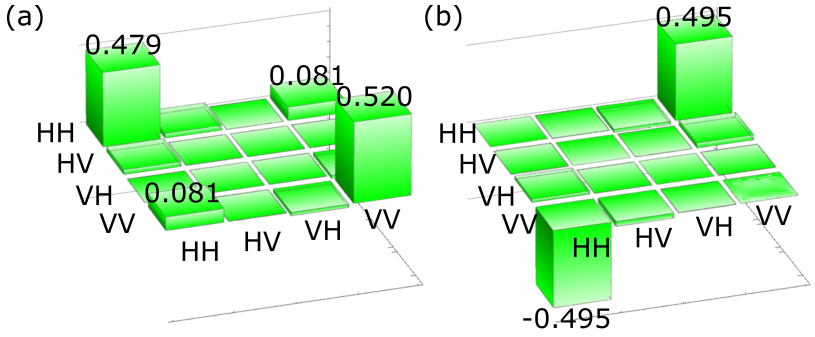

Figure 23: Reconstructed process matrix of a quarter waveplate oriented in its optical axis: real (a) and imaginary (b) parts of the Choi matrix. The measurement was performed with LC unit 2 on state preparation and LC unit 1 on analysis. Purity and fidelity of this process are $P_{\mathrm{QWP}} = 1.000$ and $F_{\mathrm{QWP}} = 0.995$, respectively

time spent by preparing the state. Conventional rotation of waveplates takes time in order of seconds to prepare one polarization state. If one wants to perform a conventional full process tomography of an $N-$qubit system, it requires 6^{2N} polarization state preparations consisting of a rotation of at least one waveplate. The time spent by waveplate movement then depends on a type of used rotation stages. Two types of motorized rotation stages are available in our laboratory, the "slow" rotation stage (Newport SR50CC), and the "fast" one (Newport PR50CC).

Every polarization state analysis requires at least one 45° rotation. The "fast" stage does this movement in approximately 5 s. For 6 reconstructed states, it is 30 s spent by preparing only this projection. In total, if one uses 4 "fast" motorized stages, the time spent only by waveplate rotation is about 35 s. Experiments presented in this chapter used both types of rotation stages. QWP1, HWP1, and HWP2 were placed in the "slow" motorized

stage and QWP2 was placed in the "fast" stage. In this configuration, the time spent by waveplate movement in the measurement of each polarization state was about 50 s. The total time spent by waveplate movement during process tomography was approximately 300 s. If one uses minimal state tomography with all rotating waveplates in "fast" stages, the movement time would be at least 25 s.

On the other hand, LC modules prepare each polarization states in time that is given by the response time of the LC module. The response time is dependent on many factors, such as temperature, thickness of the LC layer, and material properties of the LC (elastic constants, dielectric anisotropy etc.) [50–52]. The main reason for response of LC on voltage changes is relaxation time of LC [51]. It also depends on the transition between two voltage levels applied on each LC module. This time is different for transitions from lower voltages to higher and for opposite voltage changes. The response is usually faster when going from lower voltages to voltages higher than half-wave voltage [53]. For that reason, the transition times of switching between two states were measured for TN LC unit 1. These results are in Tab 6.

Final state → / Initial state ↓	Ψ_1	Ψ_2	Ψ_3	Ψ_4
Ψ_1	-	164	252	948
Ψ_2	146	-	216	952
Ψ_3	110	40.8	-	500
Ψ_4	126	190	238	-

Table 6: Measured transition times when switching between two states of tetrahedron created by LC PA unit 1. Time in ms.

Using Tab. 6, we can determine the optimal sequence of the measurement to further shorten the time required for the polarization state tomography. In this case, the optimal sequence of measurements would be $\Psi_4 \to \Psi_3 \to \Psi_2 \to \Psi_1$ giving minimal time $t \approx 425$ ms, which is approximately 2 times faster than inverse sequence, used in these measurements. However, the response time can be further compressed.

There are several methods to shorten the response times. Most of the techniques are based on applying some other field to the LC. One approach also uses magnetic field to shorten the response time [54]. However, the most used method for improving the response time uses the transient nematic effect [50, 51]. The basic idea is to apply maximal ("over-

shoot") or minimal ("undershoot") voltage for a short time before applying the required voltage [50, 53].

In a case of minimal process tomography, 4^{2N} measurements are performed. For 1 qubit, it is 16 measurements and 20 state preparations (4 prepared polarization states and 4×4 states in polarization state analysis). Total time spent by measurement of one polarization state was approximately 4.2 s. Duration of process tomography, achieved in presented experiments, is about 17 s. This time includes polarization state preparations, reading the data from the multimeter, and time of the ML reconstruction procedure. Projection intensities were read out of the TTi 1906 multimeter. It is possible to read $3 - 4$ data samples per second from this instrument. For each projection, 2 data samples were read out. The total time spent by data acquisition in process analysis was $16 \cdot 0.66 \doteq 10.6$ s. The residual time (≈ 2.6 s) was saved as a reserve. The time spent by polarization state preparation and analysis is comparable with the data acquisition time. However, if projections were measured in optimal order, the time for polarization state reconstruction can be reduced by roughly 2 s and duration of process reconstruction can be reduced by 5 s. The transient nematic effect can make the measurement even faster.

In typical quantum optics experiment with single photons, the 20 mW of laser power provides approximately $2.9 \cdot 10^6$ coincidences/s. Usual setup (quantum gate) has transmissivity for coincidences $\frac{1}{100}$. In total, at the output, we obtain roughly $29 \cdot 10^3$ coincidences/s. For successful polarization state tomography, we typically need at least 100 coincidences in maximum. This gives minimal acquisition time 3.4 ms. Because the average response time of the LC PA unit 1 in optimal configuration is about 170 ms, we can extend the data acquisition time. If we set data acquisition time to 100 ms , we can obtain about 2900 coincidences in maximum and thus, increase the precision of polarization state reconstruction, while keeping the total time short.

In this chapter, I have shown that TN LC modules can be used for polarization state preparation and analysis. This technique, in comparison with the traditional method based on rotating waveplates, has several advantages. The first one is the speed of the measurement. The second advantage is that there is no physical movement of any element and all changes of polarization states are caused by voltage changes. Therefore, problems such as precession of beam due to imperfections of moving waveplates are removed.

Two configurations of LC PA units were constructed. The first LC PA unit was built with two TN LC modules. This unit is cheap, however, rotated configuration (see Fig. 15)

means that it has to be adjusted in the experimental setup with high precision to avoid the beam passing partially out of the intersection of active segments. This kind of PA unit can be used only for one beam. The second LC PA unit uses configuration with horizontally oriented, parallel aligned segments with QWP between LC modules. The main advantage of this configuration is that it is relatively simpler to adjust in the experiment because only vertical alignment of the two segments is crucial (see Fig. 18). It also enables propagating two beams through one segment, making this unit usable in applications, where two close parallel beams are present.

6 Polarization filter

Polarization filters serve to selectively attenuate one polarization component of entering light. They could be found in many quantum optics experiments, e.g., orthogonalization of unknown states [55], quantum control phase gate [56], and in remote state preparation [57]. The polarization filter can find application also in optical attenuators [58] and shutters [59] for amplitude modulation. This setup is also used for switching between two paths [60]. Most of referenced articles show construction of these devices with LC modules. Polarization filters are usually built using polarization Mach-Zehnder interferometer. *K. Fischer et. al.* built an single qubit depolarizing channel using fast polarization changes provided by LC modules placed in an polarization interferometer [61].

6.1 Polarization interferometer

Polarization interferometers are usually used in applications that require transcription between polarization and spatial encoding of information and in applications that require long term stability. These are reasons why inherently stable polarization Mach-Zehnder interferometers are constructed. The basic principle of the interferometer could be described as follows. The incident beam enters the calcite polarization beam displacer. Its optical axis is oriented at some angle ξ. The horizontal polarization feels extraordinary refractive index n_{e}, while vertical polarization feels ordinary refractive index n_{o}. This birefringence causes the spatial separation of the two polarisation components of the incident light. The distance between the two paths is determined by the length of the calcite crystal.
The two separated paths are then combined back together on the second beam displacer. To achieve this, the half-waveplate oriented at 45° in respect to its optical axis is present in the setup, changing the horizontal polarization into vertical and vice-versa. The two beams then interfere on following polariser. Phase in the interferometer can change by tilt of calcite beam displacers.
The scheme of polarization Mach-Zehnder interferometer is depicted in Fig. 24. Calcite beam displacers used in following experiments separate H and V beams by 4 mm.

6.2 Polarization filter with one LC module

The polarization filter was built using the polarization Mach-Zehnder interferometer. The experimental setup is schematically depicted in Fig. 25.

Figure 24: Scheme of the polarization Mach-Zehnder interferometer: beam displacer (BD), half waveplate (HWP), polarization state preparation (P), polarization state analysis (A). The separation between the two paths is 4 mm

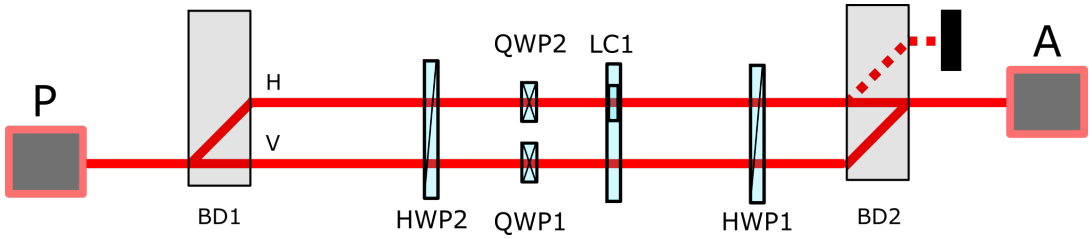

Figure 25: Scheme of polarization filter with one TN LC module: polarization state preparation (P), polarization state analysis (A), beam displacer (BD), half waveplate (HWP), quarter waveplate (QWP), LC - liquid crystal module

One LC module was added to the Mach-Zehnder interferometer. The LC module was arranged that one path of the interferometer was passing through the segment of the module, so its polarization state is changed with varying voltage. The second path passes through voltage independent area (off-segment). The filtration procedure than works as follows. The initial polarization (D) is spatially decomposed into H and V parts on the BD1. H polarization in the upper arm of the interferometer is changed to D and in the lower arm from V to A by HWP2 rotated by 22.5° to its optical axis. Lower path then propagates through QWP1 and the off-segment area of the LC module (LC1). These together transform A polarization to D. The light in the lower path then propagates through HWP1 oriented at 22.5° to its optical axis and rotates the polarization state from D to H. Light in the upper path after HWP2 propagates through segment of the LC module. The QWP2 before LC module serves to preserve interference by compensating the path difference between upper and lower arm. Then it passes through HWP 1 and vertical part of the polarization is recollected with light propagated in lower arm. For maximal voltage applied to the LC module (10 V_{pp}), the polarization of upper path does not change and HWP1 rotates the D polarization to H and it is displaced by the BD2, causing that the light does not recollect with the lower path. If lower voltage is applied to the LC1, the

amount of light from upper path recollected with light from lower path, increases. When LC1 switches D to A, all the light from upper path is recollected and the output state is the same as input state. This experimental setup was evaluated by the means of full process tomography. To illustrate the action of the polarization filter, the filtration of D polarization state for various voltages applied to the LC module is depicted in Fig. 26.

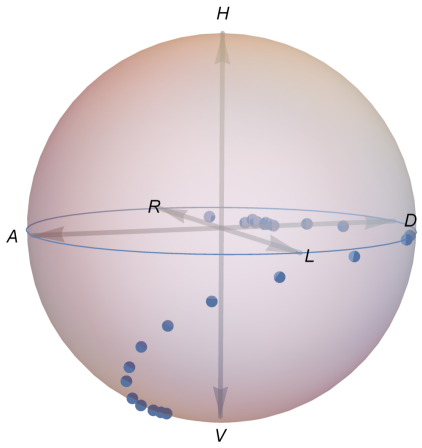

Figure 26: Polarization state (blue markers) as a function of applied voltage.

As we can see in Fig. 26, the polarization state detected on the output detector varies with voltage applied on the LC module. Until reaching certain voltage, the polarization state travels along the equator of the Poincare sphere. This means, that for these voltages, only a phase is modulated with increasing voltage. After reaching the threshold voltage, the polarization filtration begins. The polarization in upper arm of the interferometer is changed by the LC module with applied voltage. With increasing voltage, the output polarization approaches the V state.

The advantage of this polarization filter realization is its relative simplicity. The filter uses the inherently stable Mach-Zehnder interferometer for transcription of polarization degree of freedom into spatial degree of freedom. The filtration itself is then performed by applying voltage on one LC module. However, this relatively simple experiment has disadvantage. The trajectory of the output polarization state dependent on voltage applied to the module, does not change along the "meridian", but it moves along more complicated curve. This causes that additional phase shift has to be taken into account in possible applications.

The average visibility in this experiment was $(96.7 \pm 0.3)\%$. This is a good value because the detection was placed directly after the polarization state analysis. At the same time,

It shows that even LC modules based on LC displays with no advanced precision for laboratory use can be used in interferometric experimental setup and does not make drastic deformations of a wavefront.

In this section I have shown, that tunable filtration could be achieved with a simple LC module accompanied with 2 "compensation" QWPs. Maximal filtration in this case is very high, however the polarization state transformation is not simple. The additional phase shift is added during the process of filtration. The advantage of this experimental setup is its simplicity, good stability, and speed of state transformation.

7 Tunable phase modulator

Phase modulation is a useful tool in quantum optics and quantum information experiments. The phase change is a core of quantum CZ gate, which belongs to a set of basic quantum logic gates.

The tunable phase modulator with two LC modules was constructed using the polarization Mach-Zehnder interferometer. One path of the interferometer propagated through in-segment regions of the LC modules, while the second path passed through two off-segment regions, as illustrated in the scheme of the experiment in Fig. 27.

Between the two LC a HWP oriented at 45° in respect to its optical axis modules is

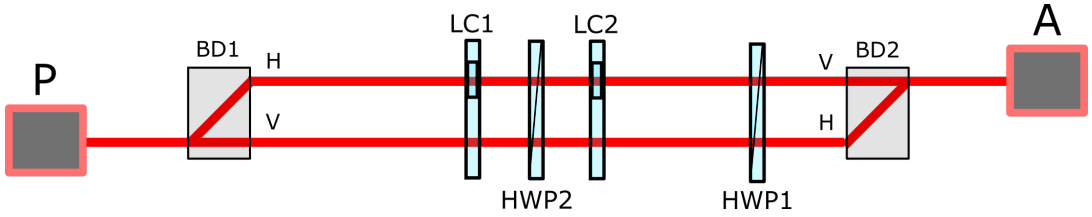

Figure 27: Scheme of polarization filter with 1 LC module: P - polarization state preparation; A - polarization state analysis; BD - beam displacers; HWP - half-waveplate; QWP - quarter-waveplate; LC - liquid crystal module.

placed. This causes, that while the "lower" path of the interferometer feels fixed phase chnge, the phase change of the "upper" path of the interferometer depends on the voltages applied on the two LC modules. Because the voltage dependences of LC1 and LC2 are shifted, voltage applied to LC1 satisfies $V_{\mathrm{LC1}} = (V_{\mathrm{LC2}} - 0.17)\ \mathrm{V_{pp}}$. Further in this chapter, the mentioned voltages will correspond to V_{LC2}. To illustrate the results of this experiment, the output polarization state is depicted in Fig. 28.

If phase between the horizontal and vertical polarization is changed, the polarization state, measured at the output of the experiment (part "A" in Fig. 27), changes only along the equator of the Poincare sphere. If polarization state in one path changes, the balance between H and V would not be preserved and the experimental setup would work as polarization filter described in Sec. 6. If one state would be filtered, the trajectory of polarization state would not go exactly along the equator, but proceed towards H or V state on the Poincare sphere. However, this is not present in this experimental setup and we can say, that phase modulator was created. Fig. 28 clearly shows that the output polarization state follows the equator of the Poincare sphere. The whole equator is not

covered due to maximal retardance of the used module, that is smaller than 2π. Red dots in Fig. 28 represent 7 states on equator of Poincare sphere prepared by waveplates (the stage P in Fig. 27).
The average visibility during these measurements was 95%. This means, that visibility decreased by approximately 1.5% when second LC module was inserted into the interferometer.

This experimental setup could be used to prepare an arbitrary state on the equator of the Poincare sphere. For example one can prepare 4 of 6 basis states (D, A, R and L) and switch between them very fast.

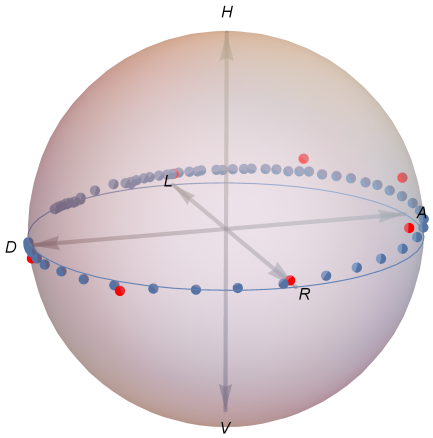

Figure 28: Output polarization states (blue dots) after propagating through a setup working as phase modulator. Solid blue circle represents equator of the Poincare sphere. Red dots stand for polarization states prepared by rotating waveplates.

8 Polarization filter with phase modulator

For experiments, it is usually good to be able to perform filtration along meridian of the Poincare sphere. The advantage of this configuration is that it does not add any additional phase shift. The filter presented in previous Sec. 6.2 does not provide such transformation, as the trajectory on the Poincare sphere is not simple. The "meridian" trajectory can be achieved by combining the simple filter setup presented in Sec. 6 and phase modulator, presented in Sec. 7. The experimental procedure of filtration along meridian of the Poincare sphere then requires at first stage applying filtration of filter and compensation of the unwanted phase shift with the phase modulator.

The scheme of this setup is shown in Fig. 29. The light from laser diode is guided through a PM fibre to collimator where it is decoupled. Then the polarization state is prepared by propagating through a polariser and a sequence of HWP and QWP (part P in Fig. 29). When the polarization state is prepared, its H and V parts are spatially separated at the BD1. Then the light enters the phase-modulation part of an experiment. The necessary phase shift between the two beams for compensation of the non-trivial action of the simple filter is applied by setting proper voltage on LC modules 1 and 2 (LC1, LC2). The filtration part then works exactly the same as presented in Sec. 6. The process of

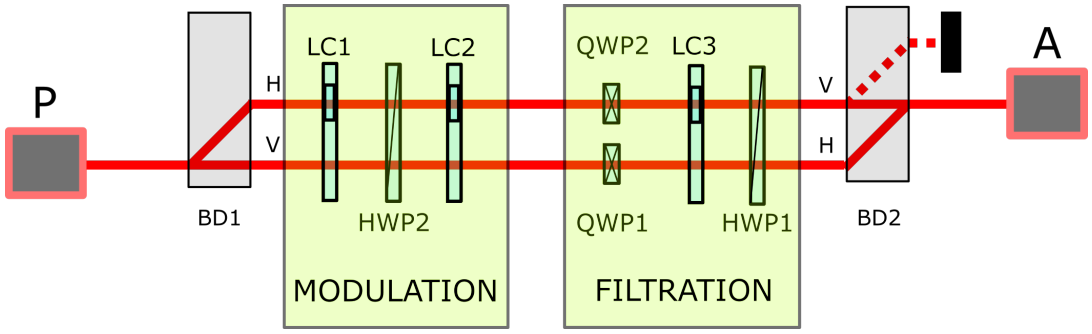

Figure 29: Scheme of the filter with combination with phase modulator: polarization state preparation (P), polarization state analysis (A), beam displacer (BD), half waveplate (HWP), quarter waveplate (QWP), liquid crystal module (LC)

finding the proper phase modulation for achieving the "meridian" trajectory was done as follows. Let us have polarization state $|\Psi\rangle$ placed on the equator of the Poincare sphere. We want to apply filtration of this state along meridian that passes through this state $|\Psi\rangle$. First, we set proper voltage on filtration LC module. Then, on analysis stage of the experiment (part A in Fig. 29, the projection onto $\left|\Psi^{\perp}\right\rangle$ is set. In the next step, the

minimum of intensity is found by varying voltages applied to the modulation part of the experiment. As we can see in Fig. 30, this method works better for states closer to the equator of the Poincare sphere. The reason for this is that with closing to the pole of the Poincare sphere, the projections onto state on the equator is closer to $\frac{I_{\max}}{2}$ and varies less with changing phase modulation. This causes, that in some case the minimum could be fund for another voltage due to intensity fluctuations.

The visibility during this experiment was 99%. The improvement in comparison with the previous experiments is due to coupling into the single mode fibre, after propagating through polarization state analysis. This is a good result because the slight wavefront distortion caused by multiple LC modules could be removed.

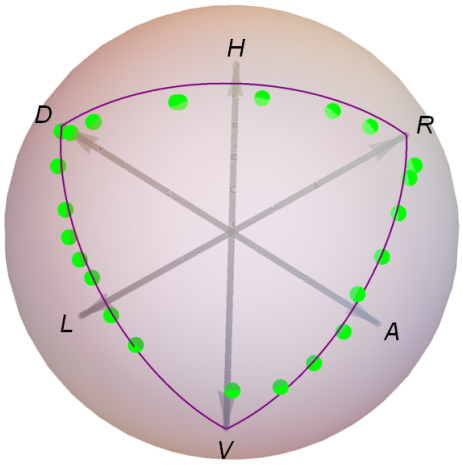

Figure 30: States achieved achieved with the combination of phase modulator and filter. Green dots represent measured data. Purple arcs represent parts of meridians (arcs going from D or R to V) and equator (arc connecting D and R) of the Poincare sphere.

Fig. 30 shows that the output polarization state changes along the meridians of the Poincare sphere. We can choose, which meridian trajectory the polarization state follows by setting proper projection when finding minimum during the phase-compensation procedure.

The filtration could be "turned off" and the experimental setup can work as phase modulator (part of the trajectory along the equator in Fig. 30).

The phase-compensated filter was created by combining the experimental setup of phase modulator (Sec. 7) and simple filter (described in Sec. 6. Using this configuration, the trajectory along the meridian was achieved. Further more, the polarization modulator allows us to perform filtration along any meridian of the Poincare sphere simply by applying proper voltage onto the phase modulator. The big advantage of this experimental realization of polarization filter is its simple application in experiments that work with polarization filters. During implementation of this method, only calibration consisting of finding proper voltages for modulation and filtration need to be found. Another advantage is the speed. Once the filtration voltages are found, these stay constant during measurement, thanks to inherently stable Mach-Zehnder interferometer. The relative disadvantage of this experimental setup is its complexity, as it consists of 3 LC modules, 2 QWPs and 1 HWP. This requires relatively long construction time and high precision during adjusting components in the experiment.

Conclusion

In this Thesis, I have worked with twisted nematic liquid crystal devices, based on LC displays commonly used in applications, such as calculators, digital watches etc. Results of my experiments show that even this kind of elements can find use in quantum optics experiments. They can find application in polarization filters, or as phase modulators. Great application of these elements is in polarization state preparation and analysis, where they can replace standard quarter and half waveplates. In these experiments, they provide us faster measurements with the same or better output qualities as conventional methods.

Polarization state preparation performed in Sec. 5 used LC PA units to perform the minimal qubit state tomography. Two LC PA units were assembled. First, unit contains two LC modules. This unit and its scheme are depicted in Fig. 15. By applying proper voltages, optimal tetrahedron for minimal quantum state tomography, with volume $V_{\mathrm{tet1}} = 0.998\ \mathrm{V_{opt}}$, has been found. This unit has been used to perform the tomography of polarization states. Results of this experiment are in Tab. 4. Later, second unit (LC PA unit 2) has been assembled. Its photo and scheme are depicted in Fig. 18. The optimal tetrahedron created by this unit has been found and in combination with LC PA unit 1, it was used to perform the process reconstruction. The reconstructed matrix of a process of a free space is depicted in Fig. 21. All the results show that polarization state preparation and analysis using LC modules work sufficiently well and parameters describing the quality of measurements, such as fidelity and purity, are the same or slightly better than ones obtained by conventional methods. Using the LC method the total time of tomography of process ≈ 17 s has been achieved. At the end of this section, the effect of the response time of LC modules on measurement duration has been discussed and steps for optimization of the measurement time have been proposed. These consist of optimization measurement ordering and more complex methods of driving LC modules.
Experiments presented in Sec. 6, Sec. 7, and Sec. 8 use LC modules in inherently stable polarization Mach-Zehnder interferometer. In different experiments, up to three LC modules were present in the experimental setup. The visibility of the interferometer decreased by approximately 1.5% with each LC module. The perfect visibility 99% has been restored when the output was coupled into single mode optical fibre.

Polarization filter in inherently stable Mach-Zehnder interferometer has been presented in Sec. 6. The filtration is determined by voltage applied on the LC module. For further improvements, two QWPs have been added to the experimental setup. The result of this

experiment is depicted in Fig. 26. This kind of filter can find applications in amplitude modulators, however, faster methods ,such as Pockels cells would be more suitable for this purpose, as they are faster. In applications, such as arbitrary state orthogonalization or qubit transfer, the additional phase shift would have to be taken into account.

The tunable phase modulator has been introduced in Sec. 7. It works in polarization Mach-Zehnder interferometer and the phase shift between horizontal and vertical polarization has been realised using two LC modules. One path of the interferometer passes through active segment area of two modules, while the second path goes through area of display that is not affected by applied voltage. HWP oriented at 45° to its optical axis was placed between the two LC modules to obtain the phase-only transformation. The result of this experiment is depicted in Fig. 28.

Last experiment presented in this Thesis combines the phase modulator presented in 7 and filter presented in 6. This experiment has been described in Sec. 8. The combination of the two "devices" works as polarization filter, which does not add any phase shift. This is shown in Fig. 30. Using this experimental setup, we can perform filtration, phase modulation or both operations at once. This gives us universal tool for preparing any polarization state on one hemisphere of the Poincare sphere.

Experiments presented in this Thesis can find applications in a broad spectrum of quantum information experiments. Every quantum gate working with qubits encoded into polarization degree of light, can use TN LC units for polarization state preparation and analysis. The time consumption of either polarization state preparation and analysis could be reduced by factor of 3 relative to currently used standard methods. This opens possibility to perform experiments that require very long time, thus can not be performed at the moment. Units presented in this Thesis will be used in our laboratory to measure entanglement of two photons in the newly constructed source of entangled photons.
Phase modulators made with LC modules, as presented in this Thesis, can be used in experiments dealing with adaptive quantum state discrimination, where they can switch measurement basis on the equator of polarization state in a real time by including proper feed-back.

References

[1] J. L. O'Brien, Science **318**, 1567 (2007).

[2] H. Häffner, C. Roos, and R. Blatt, Phys. Rep. **469**, 155 (2008).

[3] P. Kok, W. J. Munro, K. Nemoto, T. C. Ralph, J. P. Dowling, and G. J. Milburn, Rev. Mod. Phys. **79**, 135 (2007).

[4] J. Clarke and F. K. Wilhelm, Nature **453**, 1031 (2008).

[5] D. P. DiVincenzo, Fortschritte der Physik **48**, 771 (2000).

[6] E. Knill, R. Laflamme, and G. J. Milburn, Nature **409**, 46 (2001).

[7] H. Takesue, S. D. Dyer, M. J. Stevens, V. Verma, R. P. Mirin, and S. W. Nam, Optica **2**, 832 (2015).

[8] X.-M. Jin, J.-G. Ren, B. Yang, Z.-H. Yi, F. Zhou, X.-F. Xu, S.-K. Wang, D. Yang, Y.-F. Hu, S. Jiang, T. Yang, H. Yin, K. Chen, C.-Z. Peng, and J.-W. Pan, Nat Photon **4**, 376 (2010).

[9] B. Hensen, H. Bernien, A. E. Dreau, A. Reiserer, N. Kalb, M. S. Blok, J. Ruitenberg, R. F. L. Vermeulen, R. N. Schouten, C. Abellan, W. Amaya, V. Pruneri, M. W. Mitchell, M. Markham, D. J. Twitchen, D. Elkouss, S. Wehner, T. H. Taminiau, and R. Hanson, Nature **526**, 682 (2015).

[10] A. Elhalawany and M. Leuenberger, in *APS Meeting Abstracts*, Vol. 1 (2013) p. 27013.

[11] A. Orieux, L. Sansoni, M. Persechino, P. Mataloni, M. Rossi, and C. Macchiavello, Phys. Rev. Lett. **111**, 220501 (2013).

[12] D. S. Naik, C. G. Peterson, A. G. White, A. J. Berglund, and P. G. Kwiat, Phys. Rev. Lett. **84**, 4733 (2000).

[13] J. Kempe, Contemporary Physics **44**, 307 (2003).

[14] A. M. Childs, Phys. Rev. Lett. **102**, 180501 (2009).

[15] Y.-y. Zhao, N.-k. Yu, P. Kurzyński, G.-y. Xiang, C.-F. Li, and G.-C. Guo, Phys. Rev. A **91**, 042101 (2015).

[16] K. Hirabayashi, Appl. Opt. **44**, 3552 (2005).

[17] I. Moreno, J. L. Martínez, and J. A. Davis, Appl. Opt. **46**, 881 (2007).

[18] Z. Zhuang, S.-W. Suh, and J. S. Patel, Opt. Lett. **24**, 694 (1999).

[19] L. Dupont, J. L. Tocnaye, M. Gadonna, and T. Sansoni, Ann.Télécommun. **58**, 1364.

[20] M. Baranek, P. Bouchal, and Z. Bouchal, in *Digital Holography & 3-D Imaging Meeting* (Optical Society of America, 2015) p. DW2A.12.

[21] C. Kohler, X. Schwab, and W. Osten, Appl. Opt. **45**, 960 (2006).

[22] J. Běhal, *Charakteristika činnosti prostorového modulátoru světla*, Diplomová práce, Univerzita Palackého v Olomouci, Přírodovědecká fakulta, Olomouc (2015).

[23] B. E. A. Saleh and M. C. Teich, *Fundamentals of photonics*.

[24] P. Malý, *Optika*, Vol. 1 (Praha, 2008).

[25] D. Goldstein, *Polarized Light* (CRC Press, 2003).

[26] R. C. Jones, J. Opt. Soc. Am. **31**, 488 (1941).

[27] P. Kok and B. W. Lovett, *Introduction to Optical Quantum Information Processing*, Vol. 1 (Camebridge University Press, 2010).

[28] D. F. V. James, P. G. Kwiat, W. J. Munro, and A. G. White, Phys. Rev. A **64**, 052312 (2001).

[29] J. Altepeter, E. Jeffrey, and P. Kwiat, "Photonic state tomography," in *Advances In Atomic, Molecular, and Optical Physics*, Vol. 52, edited by P. Berman and C. Lin (Academic Press, 2005) pp. 105 – 159.

[30] M. Ježek, J. Fiurášek, and Z. Hradil, Phys. Rev. A **68**, 012305 (2003).

[31] K. Banaszek, G. M. D'Ariano, M. G. A. Paris, and M. F. Sacchi, Phys. Rev. A **61**, 010304 (1999).

[32] Z. Hradil, J. Řeháček, J. Fiurášek, and M. Ježek, "Quantum state estimation," (Springer Berlin Heidelberg, Berlin, Heidelberg, 2004) Chap. 3 Maximum-Likelihood Methodsin Quantum Mechanics, pp. 59–112.

[33] J. L. O'Brien, G. J. Pryde, A. Gilchrist, D. F. V. James, N. K. Langford, T. C. Ralph, and A. G. White, Phys. Rev. Lett. **93**, 080502 (2004).

[34] J. F. Poyatos, J. I. Cirac, and P. Zoller, Phys. Rev. Lett. **78**, 390 (1997).

[35] I. L. Chuang and M. A. Nielsen, J. Mod. Opt. **44**, 2455 (1997).

[36] M. W. Mitchell, C. W. Ellenor, S. Schneider, and A. M. Steinberg, Phys. Rev. Lett. **91**, 120402 (2003).

[37] J. Fiurášek and Z. Hradil, Phys. Rev. A **63**, 020101 (2001).

[38] H. Kawamoto, Proceedings of the IEEE **90**, 460 (2002).

[39] S. H. Perlmutter, D. Doroski, and G. Moddel, Appl. Phys. Lett. **69** (1996).

[40] D.-K. Yang and S.-T. Wu, "Optical modeling methods," in *Fundamentals of Liquid Crystal Devices* (John Wiley & Sons, 2014) pp. 87–125.

[41] A. Yariv and P. Yeh, *Optical waves in crystal propagation and control of laser radiation* (John Wiley & Sons, 1983).

[42] P. Yeh and C. Gu, *Optics of liquid crystal displays*, Vol. 67 (John Wiley & Sons, 2010).

[43] D.-K. Yang, *Fundamentals of liquid crystal devices* (John Wiley & Sons, 2014).

[44] A. Vargas, R. Donoso, M. Ramírez, J. Carrión, M. Sánchez-López, and I. Moreno, Optical Review **20**, 378 (2013).

[45] ThorLabs, "LCC Retarders Performance Data," (2006).

[46] V. Krčmarský, "Polarization state control using liquid crystals (bachelor thesis)," (2014).

[47] J. Řeháček, B.-G. Englert, and D. Kaszlikowski, Phys. Rev. A **70**, 052321 (2004).

[48] A. Peinado, A. Lizana, J. Vidal, C. Iemmi, and J. Campos, Appl. Opt. **50**, 5437 (2011).

[49] A. Ling, K. P. Soh, A. Lamas-Linares, and C. Kurtsiefer, Phys. Rev. A **74**, 022309 (2006).

[50] S. Wu and C. Wu, J. Appl. Phys. **65** (1989).

[51] I.-C. Khoo and S.-T. Wu, *Optics and nonlinear optics of liquid crystals*, Vol. 1 (World Scientific, 1993).

[52] R. I. McCartney, in *SID Symposium Digest of Technical Papers*, Vol. 34 (Wiley Online Library, 2003) pp. 1350–1353.

[53] Meadowlark Optics, Inc, "Response time in liquid-crystal variable retarders," `http://www.meadowlark.com/store/applicationNotes/Response%20Time%20in%20Liquid%20Crystal%20Variable%20Retarders.pdf`, Meadowlark Optics material; Accessed: 2016-04-22.

[54] B. Wang, X. Wang, and P. J. Bos, J. Appl. Phys. **96** (2004).

[55] M. Ježek, M. Mičuda, I. Straka, M. Miková, M. Dušek, and J. Fiurášek, Phys. Rev. A **89**, 042316 (2014).

[56] K. Lemr, A. Černoch, J. Soubusta, K. Kieling, J. Eisert, and M. Dušek, Phys. Rev. Lett. **106**, 013602 (2011).

[57] N. A. Peters, J. T. Barreiro, M. E. Goggin, T.-C. Wei, and P. G. Kwiat, Phys. Rev. Lett. **94**, 150502 (2005).

[58] G. Zhu, B. yan Wei, L. yu Shi, X. wen Lin, W. Hu, Z. di Huang, and Y. qing Lu, Opt. Express **21**, 5332 (2013).

[59] N. Spagnolo, C. Vitelli, S. Giacomini, F. Sciarrino, and F. D. Martini, Opt. Express **16**, 17609 (2008).

[60] N. A. Riza, Opt. Lett. **19**, 1780 (1994).

[61] K. A. G. Fisher, R. Prevedel, R. Kaltenbaek, and K. J. Resch, New J. Phys. **14**, 033016 (2012).